Effect of Charge Exchange on 2D Hall Thruster Simulation

Article · January 2005

3 authors, including:

Nicolas Gascon
Stanford University
67 PUBLICATIONS **1,003** CITATIONS

Eduardo Fernández
20 PUBLICATIONS **140** CITATIONS

Some of the authors of this publication are also working on these related projects:

Plasmic Thruster View project

Observatório Latino Americano de Arboviroses (LACONDE) View project

Effect of Charge Exchange on 2D Hall Thruster Simulation

IEPC-2005-057

Michelle K. Allis[*], Nicolas Gascon[†], and Mark A. Cappelli[‡]
Stanford University, Stanford, CA, 94305

and

Eduardo Fernandez[§]
Eckerd College, St. Petersburg, FL, 33711

        The impact of charge exchange collisions on the interior and near-field region of a Hall thruster is examined using a two-dimensional hybrid particle-in-cell simulation in the radial-axial plane. The electrons are modeled as a quasi-one-dimensional fluid and the ions and neutrals are treated as discrete superparticles capable of motion in all three dimensions. The effect of collisions is evaluated through a careful study of the ion and neutral velocity distributions at the exit plane and in the near field region. It has been determined that while collisions have a noticeable effect on the time averaged plasma properties, the changes due to momentum transfer that occur during these collisions are not distinguishable from general fluctuations. In addition, the role of electron wall damping is examined as well as the effect of a finite background pressure in the chamber.

Nomenclature

B	=	magnetic field
e	=	electron charge
E	=	electric field
g	=	relative velocity
I_a	=	discharge current
j	=	current density
k	=	Boltzmann constant
K	=	thermal diffusivity
$m_{e,i}$	=	electron/ xenon ion mass
$n_{e,i}$	=	plasma/ ion density
n_n	=	neutral density
S	=	channel cross section
T_e	=	electron temperature
u	=	velocity
δ	=	total secondary electron emission yield
Γ_E	=	electron energy flux to wall

---

[*] Research Assistant, Mechanical Engineering, mkallis@stanford.edu
[†] Post-Doctoral Research Associate, Mechanical Engineering, Nicolas.Gascon@stanford.edu
[‡] Professor, Mechanical Engineering, cap@stanford.edu.
[§] Assistant Professor, Natural Sciences, fernane@eckerd.edu

ϕ	=	electric potential
ϕ_w	=	potential of wall relative to bulk
ϕ^*	=	thermalized electric potential
φ	=	ion production cost
μ	=	electron cross-field mobility
θ	=	polar scattering angle
σ	=	total cross section

I. Introduction

In a typical Hall thruster, electrons travel from an external cathode to an anode at the base of an annular channel. Along their path, the electrons encounter a region of high resistivity due to an imposed radial magnetic field, and become trapped in an E×B Hall current. When neutral particles injected from the anode encounter this region of high electron density, electron impact ionization occurs. The newly born unmagnetized ions then accelerate out of the thruster due to the electrostatic potential maintained between the anode and cathode. While this process results in a high specific impulse device suitable for various low thrust applications, the neutral particles which traverse the length of the channel without becoming ionized may be cause for concern. Not only do these neutral particles decrease the overall efficiency of the thruster, but collectively they form a low velocity plume of exhaust and collide with the high velocity ions. In the case of charge exchange collisions, these interactions result in slow ions scattered at large angles and increase the probability of damage to the spacecraft by sputtering and deposition.

In order to better understand the effect of charge exchange collisions on Hall thruster plasmas, these collisions are simulated in a two dimensional numerical model of a laboratory Hall discharge. The hybrid model treats the electrons as a quasi-one dimensional fluid, assuming infinite conductivity parallel to the magnetic field lines, and the xenon atoms and ions as discrete superparticles. The heavy particles and electron fluid solutions are coupled in the hybrid simulation by assuming space charge neutrality. Plasma properties are calculated using a particle-in-cell approach and compared with experimental measurements to evaluate simulation accuracy. In order to account for the anomalous electron cross field conductivity, an experimental effective Hall parameter is imposed.

To model collisions in the simulation, collision partners are chosen using a direct simulation Monte Carlo method as described by Bird[1] and total cross section data obtained from Miller et al.[2] In order to more accurately predict the velocity distribution of energetic particles, available low-energy differential scattering data for helium from Gao et.al.[3] is incorporated. Since it is assumed that elastic collisions should not significantly affect the shape of the distribution functions, momentum transfer collisions have been ignored.

In addition to summarizing the impact of charge exchange collisions on the simulation, this paper will also provide a description of the implemented numerical model. Due to the sensitivity of the simulation to electron wall interactions, prior to evaluating charge exchange, preliminary results at improving simulation output by including ad-hoc modifications to the wall damping model will be discussed. Since background gas may have a significant impact on both the neutral velocity distribution and the collision rate, the effect of background gas will also be examined.

II. Numerical Model

A. Assumptions

To aid in the understanding of Hall thruster dynamics, a two dimensional model has been constructed in the radial-axial plane[4] similar to the model described by Fife.[5,6] The hybrid model employs a quasi-one-dimensional fluid treatment of electrons and a particle-in-cell (PIC) treatment of the heavy species, Xe and Xe$^+$. Since the Debye length of a typical Hall thruster plasma is smaller than the length scales of interest, the two solutions are coupled assuming space charge neutrality. A similar model, also being presented at this conference, is currently being developed in the azimuthal-axial plane.[7]

The computational geometry used in the simulation corresponds to the laboratory discharge referred to here as the Stanford Hall Thruster, given that extensive experimental data exists for comparison purposes. The annular channel is approximately 8 cm in length and 1.2 cm in width. The insulating channel walls are made of alumina. A mass flow rate of 2 mg/s is implemented in the model to match experimental conditions.

Measurements of the magnetic field along the channel centerline are used to impose a constant external magnetic field as shown in Fig. 1. It is assumed for the results presented that the discharge does not significantly affect the shape or strength of the field. However, a quantitative study of the induced magnetic field and its affect on wall

2
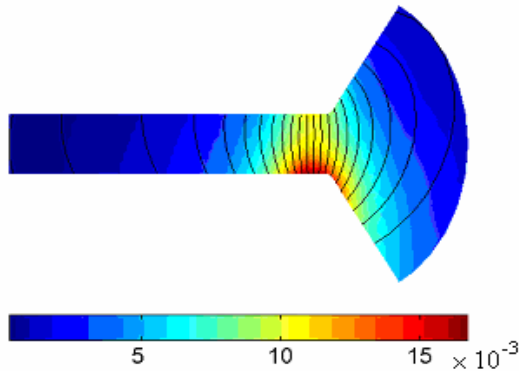
Figure 1. Magnetic field strength [Tesla] and contour lines of Stanford Hall Thruster.
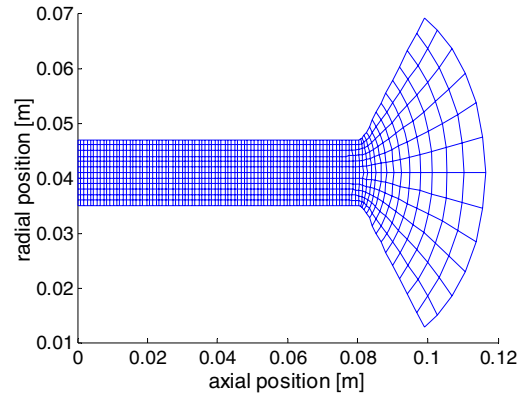
Figure 2. Computational grid of Stanford Hall thruster radial-axial simulation.

erosion is presented at this conference.[8] The radial variation of the magnetic field is obtained by solving Laplace's equation for the magnetic potential after specifying the location of the magnetic poles and assuming infinite permeability of the pole pieces. Due to high electron conductivity parallel to the field lines, the electron temperature is assumed to be uniform along magnetic contours.

B. Neutrals

Neutral xenon particles are injected from a region near the center of the anode according to a prescribed mass flow rate of 2 mg/s. The introduced particle velocity distribution is assumed to be that of a Maxwellian one-way flux[9] corresponding to the anode temperature of 1000K. Sonic injection does not significantly affect results downstream of the anode. However, diffuse injection is assumed to be more realistic and will therefore be the only injection scheme presented.

Since neutral particles are not affected by electric and magnetic fields, the magnitude and direction of velocity remain the same at each timestep, while the azimuthal and radial components of velocity are modified to account for the annular geometry. Particles which exit the computational domain along the channel walls are reflected back into the domain. It is assumed that particles that impact the channel walls thermalize at the wall temperature and are diffusely scattered back into the channel. Similar to anode injection, the velocity distribution is assumed to be half-Maxwellian. Particles which exit the computational domain in the plume region are no longer tracked by the simulation.

C. Ions

Singly-charged xenon ions are generated through electron impact ionization of neutral atoms. The ionization rate is calculated as a function of electron temperature by assuming Maxwellian electrons and using experimental cross section data reported in the Siglo database.[10] In addition to increasing the ion population, the ionization process simultaneously depletes the neutral population at each time step. In the present model, only singly-charged ions are considered.

Due to their large inertia and Larmor radius, ions are not significantly affected by the external magnetic field. Therefore, the cylindrical equations of motion used to update ion velocities at each time step only include a force due to the transient, spatially varying electric field. Ions which impact channel walls recombine to form neutrals and are scattered diffusely using a half-Maxwellian velocity distribution at 200 K. Similar to the neutral treatment, ions leave the simulation after crossing the computational boundaries in the plume.

D. Electrons

As outlined by Fife,[5,6] the electron fluid is governed by the first three moments of the Boltzmann equation in addition to a current conservation equation, assuming quasineutrality.

Neglecting inertial terms and collisional effects, the momentum equation parallel to the magnetic field describes a balance between electric and pressure forces. Integrating along an isothermal magnetic contour yields an expression for the electric potential, ϕ.

The 29th International Electric Propulsion Conference, Princeton University,
October 31 – November 4, 2005

$$\phi = \frac{kT_e}{e} \ln(n_e) + \phi* \qquad (1)$$

where ϕ^* is the thermalized electric potential, k is the Boltzmann constant, e is the charge of an electron, T_e is the electron temperature, and n_e is the plasma density. The electric field, E, is then given everywhere in the domain by:

$$E = -\nabla \phi \qquad (2)$$

Perpendicular to the magnetic contours, the electron momentum equation balances electric, pressure, and collisional drag forces. Once again, inertial terms are ignored. An **E**×**B** axial force produced by azimuthal electric potential fluctuations interacting with the radial magnetic field is not directly captured in the 2-D simulation. However, this additional contribution to axial force is included through an effective experimental mobility and diffusivity in the generalized Ohm's law[11]:

$$u_{e\hat{n}} = -\mu \left(E_{\hat{n}} + \frac{kT_e}{en_e} \frac{\partial n_e}{\partial \hat{n}} + \frac{k}{e} \frac{\partial T_e}{\partial \hat{n}} \right) \qquad (3)$$

where $\hat{n}$ indicates the direction normal to the magnetic field, $u_{e\hat{n}}$ is the electron velocity in the normal direction, and μ is the effective mobility. The reader is referred to a paper by Thomas et al.,[12] also presented at this conference, for a further discussion on the electron mobility.

A transient, spatially varying electron temperature is determined using the second moment of the Boltzmann equation characterizing energy transport:

$$\frac{\partial}{\partial t} \left(\frac{3}{2} n_e kT_e \right) + \frac{\partial}{\partial \hat{n}} \left(\frac{5}{2} n_e u_{e\hat{n}} kT_e - K \frac{\partial T_e}{\partial \hat{n}} \right) = -\dot{n}_e \varphi(T_e) E_i - \alpha T_e^{3/2} + j_{e\hat{n}} E_{\hat{n}} \qquad (4)$$

In the above expression, K is the thermal diffusivity, which incorporates the anomalous electron transport coefficient through the measured mobility. The terms on the right hand side of Eq. (4) represent the ionization and wall damping sink terms and the joule heating source term. The ion production cost, $\varphi(T_e)$, is fit using an exponential expression given by Dugan et al.,[13] and is evolved in the original nonlinear form. The term $\alpha T_e^{3/2}$ represents the energy loss due to the electron flux to the wall.

Presently, the wall damping model is based on an energy dependent secondary electron emission yield assuming alumina walls. As described by Barral et al.,[14] the energy dependence is assumed to be linear with an asymptotic total electron emission yield of 0.57 for alumina and a crossover energy of 18 eV. If the electron distribution is assumed to be Maxwellian and isotropic, then the average energy of an electron capable of overcoming the sheath barrier is given by: $2kT_e+e\phi_w$, where ϕ_w is the difference between the bulk potential and the wall potential. Accounting for the deceleration that occurs when an electron impacts the channel wall, the total electron emission yield is therefore given by:

$$\delta(T_e[eV]) = 0.57 + \frac{2T_e}{18\,eV} \qquad (5)$$

The wall potential is calculated by equating the net electron and ion fluxes to the wall, where the factor of $e^{-1/2}$ is a result of applying the Bohm criteria for the ions.[15]

$$\phi_w = \frac{kT_e}{e} \ln\left(\frac{1-\delta}{e^{-1/2}} \sqrt{\frac{m_i}{2kT_e}} \right) \qquad (6)$$

As described by Barral et al.,[14] space charge saturation occurs when the electron emission yield reaches 0.98. In the space charge saturation regime, the potential is taken to be:

$$\phi_w = 1.02 \frac{kT_e}{e} \tag{7}$$

Once the wall potential has been determined, the electron flux to the wall is calculated, again assuming a Maxwellian, isotropic distribution. Following the model presented by Barral et al.[14] for the alumina channel, it is assumed that 57% of the electron wall emission consists of backscattered electrons and the other 43% is true secondary electron emission. The backscattered electrons are assumed to retain 60% of their primary energy, while the true secondaries are emitted from the wall with no initial energy. However, both populations are assumed to gain energy equal to the sheath potential when they re-enter the bulk. Therefore the net energy loss is given by:

$$\Gamma_E = e^{-1/2} n_e \sqrt{\frac{kT_e}{m_i}} \left[\delta \left(e\phi_w + (0.57)(0.6)(2kT_e) \right) - (2kT_e + e\phi_w) \right] \tag{8}$$

where n_e is the bulk electron density, and $\sqrt{(kT_e/m_i)}$ is the Bohm velocity.

Assuming space charge neutrality, the electron density is everywhere equal to the ion density, n_i. In order to enforce electron continuity, a total discharge current conservation constraint is imposed:

$$I_a = e \int_A n_e \left(u_{i\hat{n}} - u_{e\hat{n}} \right) dS \tag{9}$$

where S is the channel cross section.

Combination of Eqs. (1) through (3) and substitution into the current conservation equation yields an expression for the thermalized potential, ϕ^*, in terms of electron temperature. Therefore, by obtaining the electron temperature through direct solution of the energy equation, the spatially-varying electric field, electron velocity, and ionization rate can be calculated at each time step.

E. Solver Details

The computational domain of the simulation extends from the anode through the channel and into the near-field plume region. A non-uniform orthogonal grid is used to span the computational domain with 101 grid points in the axial direction and 13 in the radial direction, as shown in Fig. 2.

The numerical model implements a fourth order Runge-Kutta scheme to solve the electron energy equation in order to update the electron temperature perpendicular to the magnetic field at each time step. The spatial derivatives are calculated using second-order central differencing. The boundary conditions used in this implementation are Dirichlet for the electric potential at both the anode and cathode. The temperature boundary conditions are Dirichlet at the cathode assuming constant electron energy injection, and Neumann at the anode assuming infinite diffusion.

A standard leap-frog technique is employed for the time advancement of heavy particles. For computational manageability, superparticles are used to represent large groups of neutrals and ions rather than simulating individual particles. Since neutral and ion densities differ by orders of magnitude over the length of the domain, the size of the superparticles vary with both space and species. The simulation is initialized with approximately 300,000 superparticles of each heavy particle species. For the neutral particles, the equations of motion are solved analytically in three dimensions. The ion equations of motion are solved numerically using a second order Runge-Kutta scheme.

Due to the fast electron time scale relative to the ions and neutrals, the step size used for time advancement differs for each species. The ion and neutral time step is typically 25 ns, while the electron time step is 0.1 ns. Therefore, ions and neutrals are advanced in time after several electron iterations. On a 3.8 GHz Pentium 4 processor, the simulation completes 625 μs, or approximately five to ten "breathing mode" cycles, in one day.

III.   Results and Discussion

Before examining the effect of charge exchange collisions in the code, first an attempt will be made to increase the predictive capability of the simulation through modification of the electron wall damping model. Once a wall damping model has been established which provides reasonable agreement with experimental observations, the effect of background gas will be studied, since back pressure may play a significant role in evaluating the impact of

charge exchange. Lastly, the influence of charge transfer collisions on the simulated plasma properties and velocity distributions will be studied.

A. Electron Wall Damping

Before the effects of charge exchange can be critically examined, it is necessary that the simulation reasonably predict experimental measurements within experimental uncertainty. When the model is implemented as previously described, the discharge current is simulated to be less than 0.01 Amps which is more than a factor of 100 lower than the measured value of 2.7 Amps. Clearly, a discrepancy exists between the simulated physics and the actual behavior of the thruster. One possible explanation for this discrepancy is that experimental error in the measurements propagates into the experimental mobility, which is dependent on the plasma density, electric potential, and ion velocity. While the ion velocity is experimentally measured with great accuracy, due to the nature of the measurements, the plasma density and electric potential are not known with as much certainty. The greatest amount of experimental error is likely in the measured plasma density. If the experimental mobility is recalculated by lowering the plasma density in the ionization zone by no more than a factor of two, the average anode current is simulated to be 0.5 Amps or more than a factor of 50 greater than that found using the original mobility. However, since this current is still more than a factor of five lower than the experimentally measured current, there are clearly other issues that are not well-understood.

Another possible source of error is the assumption that the walls are made of pure alumina. In reality, although the channel of the Stanford Hall Thruster was machined from alumina, during operation the surfaces are coated with a black material. The exact chemical composition of the channel walls is unknown, though in addition to alumina, the surfaces likely contain traces of silica and carbon-products of oil vapor from diffusion pumps and other possible sources. The non-ideal nature of the walls may therefore lower the secondary electron emission that occurs when an electron strikes these surfaces. Therefore, instead of using alumina values, simulations were run with secondary electron emission yields varying between alumina, graphite, and silicon carbide values. If the crossover energy is moved from 18 eV to 100 eV and the asymptotic total electron emission yield is moved from 0.57 to 0.45, the simulated anode current becomes 1.6 Amps.

A third possible explanation for the discrepancy between the simulated and measured anode current is a violation of the isotropic, Maxwellian electron assumption. Only high energy electrons are able to penetrate the sheath and strike the channel surfaces. As described by Meezan et al.,[16] the energy transfer rate between electrons is not large enough to replenish the high velocity tail, resulting in a lower electron flux to the wall than predicted by a Maxwellian distribution. However, even if the flux were to remain the same, the non-Maxwellian, anisotropic nature of the electron distribution may also have a large effect on the energy lost per collision. In order for an electron to strike the wall it must have a velocity perpendicular to the wall which satisfies:

$$v_{e,\perp} > \sqrt{\frac{2e\phi_w}{m_e}} \tag{10}$$

in order to overcome the potential barrier in the sheath. It is assumed that when this particle impacts the wall, the components of velocity in the direction parallel to the wall are chosen randomly from a Maxwellian distribution and each carry with them $\frac{1}{2}kT_e$ of energy. When the electron strikes and a true secondary electron is emitted, it is assumed that the electron loses all its energy in all three directions. Therefore, when the secondary electron re-enters the bulk it carries with it exactly $e\phi_w$ of energy perpendicular to the wall and no energy in the other two directions. If this electron did not undergo any collisions between the two walls, it would strike the opposite wall and transfer almost no energy. Therefore, the actual amount of energy transferred during an electron collision with the wall is somewhere between the Maxwellian value of $2kT_e$ and 0. If we assume the average energy transferred to the wall is $0.8kT_e$ when calculating the secondary electron emission yield and net energy loss, then the simulated anode current is 1.7 Amps.
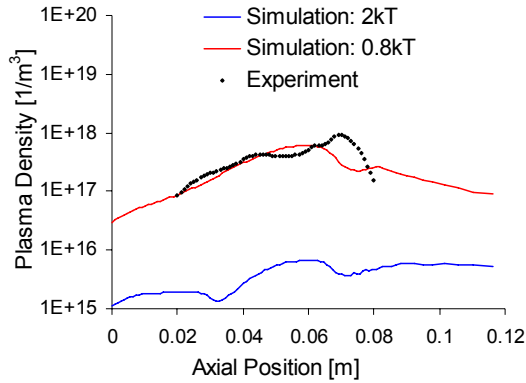
Figure 3. Comparison of experimental plasma density with simulation for electron wall collision energies of 2kT and 0.8kT.
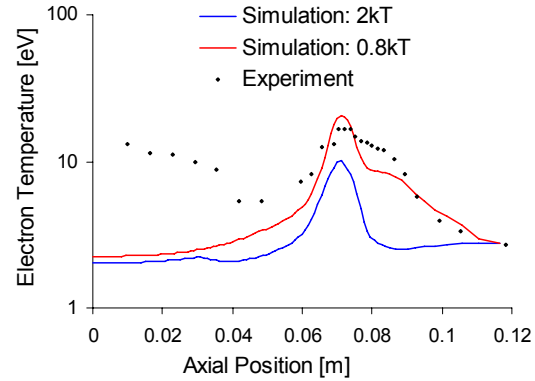

Figure 4. Comparison of experimental electron temperature with simulation for electron wall collision energies of 2kT and 0.8kT.

Each of these three mechanisms alone is not enough to explain the discrepancy between the simulated and experimental anode current. Therefore, the real reason for the difference is likely due to some combination of experimental error, non-ideal wall conditions, anisotropy, and non-Maxwellian electrons. For example, if we combine the effect of experimental error on the measured plasma density as described above with the effect of non-Maxwellian, anisotropic electrons, then the average simulated anode current is 2.6 Amps which is very close to the measured value of 2.7 Amps. However, since at present the importance of each of these mechanisms is not quantifiable, for the purposes of this paper we will simply introduce an "effective" temperature of $0.4T_e$ when calculating the electron wall damping such that the energy lost per particle is $0.8kT_e$. Although this method is no more justified than the other mechanisms for improving the anode current, by making this change the simulation predicts plasma properties with reasonable accuracy, and is sufficient, if not ideal, for analyzing the effects of charge exchange.

As shown in Figs. 3 and 4 above, by assuming the average energy lost to the wall during electron impact is $0.8kT_e$ instead of $2kT_e$, the simulation is in much better agreement with experiment. For the case of $2kT_e$ energy loss, the simulated plasma density is almost two orders of magnitude lower than experimental measurements. Near the channel exit, the simulated electron temperature is also nearly a factor of 10 too low. By lowering the average energy of an incident electron on the wall, all plasma properties can be brought to within reasonable agreement with experiment. Note that the discrepancy near the anode in the electron temperature is due to an inability of the code to capture the glow discharge in this region at 200V.

B. Background Gas

In simulations of ground-based chamber tests, the inclusion of background gas is critical in order to accurately represent the neutral number density in the very near-field of the thruster. The amount of neutral gas in the
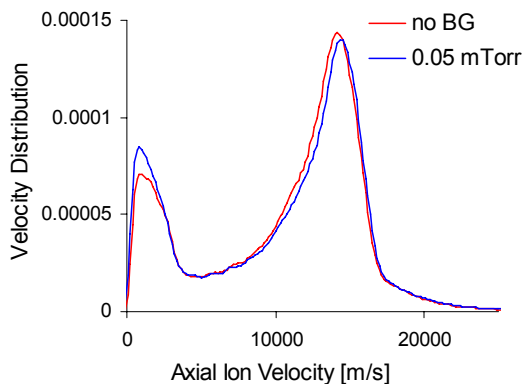
Figure 5. Comparison of axial ion velocity distribution with and without background gas 4 mm beyond exit plane of hall thruster.
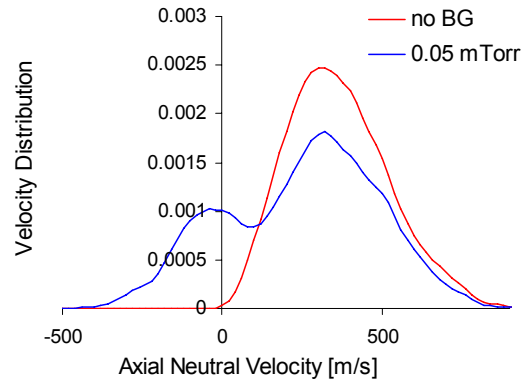
Figure 6. Comparison of axial neutral velocity distribution with and without background gas 4 mm beyond exit plane of hall thruster.

The 29th International Electric Propulsion Conference, Princeton University,
October 31 – November 4, 2005

simulation is used to calculate the ionization rate, which is directly coupled to the plasma density and electric potential. Since the quantity of slow moving neutrals is directly proportional to the number of charge exchange collisions, background pressure is also highly relevant to charge exchange analysis. In order to deduce the magnitude of background effects, simulations have been run with and without background. Addition of background gas is accomplished by uniformly injecting neutral xenon particles into the simulation from the edges of the computational domain bordering the near-field region. A net one-way flux of $n\bar{c}/4$ is assumed with a half-Maxwellian velocity distribution normal to the injection surface.

Figure 7. Comparision of experimental and simulated electric potential with simulated ionization rate along the centerline of the thruster.

Figures 5 and 6 show the effect of 0.05 mTorr of background gas on the ion and neutral axial velocity distributions along the centerline of the channel, 4 mm outside the thruster. Both distributions have been normalized. For this run, charge exchange was not included. As expected, background gas increases the population of slow moving ions, since background neutrals are more likely to get ionized at a lower potential. The average axial ion velocity at this location is lowered by 1.8 % due to the introduction of background gas. Also, background gas results in two separate populations of neutrals: those injected from anode, which have a net motion out of the thruster, and those introduced as background gas, which have a net motion into the thruster. This double hump distribution lowers the average neutral velocity by 31.8 %.

Another key feature to recognize in Fig. 5 is that even without background gas there is a significant population of low energy ions. Experimentally, as reported by Cedolin,[17] a tail of slow moving ions out to 0 m/s is observed. However, Cedolin does not measure a second local maximum at low velocities. The reason for this discrepancy is believed to be a simulated potential drop which is too steep, as shown in Fig. 7. A small amount of ionization is still occurring near the thruster exit, located 8 cm downstream of the anode. In the simulation, these newly born ions are near the bottom of the potential well and the accelerating electric field is small. However, experimentally, nearly half of the potential drop occurs outside the thruster. By the time the electric field is small, it is likely that the amount of ionization is negligible.

C. Charge Exchange Collisions

To better understand the plasma dynamics that occur inside a Hall thruster, the effect of heavy particle interactions has been studied through inclusion of charge exchange collisions. In reality, heavy particle collisions involve transfer of momentum, and in some cases, an exchange of charge. Pure momentum transfer collisions are neglected in the simulation since it is assumed that elastic collisions result in only a small change in the velocity distribution function of each species. However, since charge transfer collisions typically produce high velocity neutrals and slow moving ions, this type of collision is studied in depth. There are three cases that will be considered for comparison. In the reference case, charge exchange collisions will be neglected completely. In the second case, charge exchange collisions will be included, but the small amount of momentum transfer which occurs during these collisions will be neglected. In the most accurate case, an angular dependence of total cross section will be assumed and momentum transfer will be included. Since differential cross section data does not exist for xenon at low energies, the angular dependence of helium data[3] at 250 V will be scaled to the total cross section data for xenon.

In order to implement charge exchange collisions in the simulation, first collision partners are chosen using the pair selection scheme described by Bird.[1] Only neutrals and ions in the same computational cell are eligible to collide. From within a given cell X, ion-neutral pairs are chosen according to the formula:

$$X = n_i n_n \left(\sigma g\right)_{max} V \Delta t \tag{11}$$

where n_i is the ion density, n_n is the neutral density, $\left(\sigma g\right)_{max}$ is the maximum value of the total cross section multiplied by the relative velocity for all possible pairs, V is the volume of the cell, and Δt is the time step.

Experimental measurements by Miller et al.,[2] are used to determine the total cross section as a function of energy:
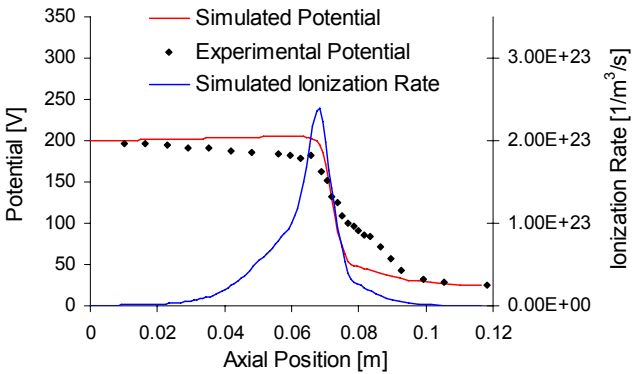
$$\sigma_{Xe-Xe^+} = \left(87.3 - 13.6 \log_{10}\left(\frac{\frac{1}{2} m_{Xe} g^2}{e}\right)\right) \times 10^{-20} \, \mathring{A}^2 \tag{12}$$

Once X partners are chosen, they are collided with probability, P, given by:

$$P = \frac{\sigma g}{(\sigma g)_{max}} \tag{13}$$

Differing superparticle weights are accounted for in selecting collision pairs. On average, a neutral superparticle is two orders of magnitude larger than an ion superparticle. Therefore, if a charge exchange collision is determined to take place, the larger particle (typically the neutral) is divided into a small particle the size of the collision partner and a large particle equal to the remainder. The collision occurs between the two equally sized particles, while the remainder particle retains its pre-collision velocity.

Since the most probable scattering event involves very little momentum transfer, for the simple case momentum transfer is neglected and the pre-collision velocities of the ion and neutral are exchanged. This will be referred to as 2D charge exchange (CEX) since the pre- and post-collision velocities can be represented in a plane.

In order to increase the accuracy of the simulation and determine the impact of the small amount of momentum transfer that occurs during a real collision, an angular probability is assumed and implemented. In the azimuthal direction, it is assumed that there is no preferred scattering direction. Therefore, the azimuthal scattering angle is chosen randomly between 0 and 2π. To obtain the polar scattering angle, θ, measured from the scattering axis, a differential cross section is constructed by scaling 250 eV helium data by Gao[3] to the total cross section of xenon given by Miller.[2] For estimation purposes, the cross section is assumed to be constant for polar scattering angles less than 0.0005 radians. For angles larger than 0.0005 radians, the low-angle helium data, which contained a number of oscillatory features, was extrapolated and approximated using a constant exponential fit such that:

$$\frac{\partial \sigma}{\partial \Omega} \propto \theta^{-2.36} \tag{14}$$

where Ω is the solid angle given by $d\Omega = 2\pi \sin\theta d\theta$. Once the assumed differential data has been normalized, the polar angle is randomly selected using a cumulative distribution function as described by Birdsall et al.[18] The energy dependence of the angular probability is neglected.

Once a collision is determined to take place and the two scattering angles are chosen, assuming conservation of energy and momentum, the collision is completely defined. Through a series of matrix operations, the coordinate system is transformed such that the ion is stationary and the trajectory of the neutral is aligned with a principal axis of the new coordinate system. The post-collision velocities are determined using the calculated angles and the inverse matrix operations are applied to transform back to the original coordinate system. In previous versions of the simulation, after a collision took place, the separated neutral particle was recombined using conservation of momentum in order to retain the original number of particles. However, in addition to resulting in a loss of energy, this method is not sufficient for analyzing the post-collision neutral velocity distribution. Results suggest recombination may also lead to a significant amount of inaccuracy, particularly in the neutral velocity. By averaging the large post collision velocity of a neutral particle with the slower neutral population, the fast particle does not leave the simulation as quickly as it should, resulting in an artificially enhanced neutral velocity in the near field region.
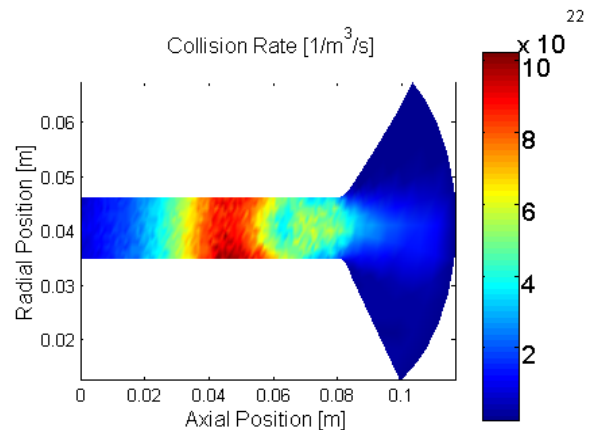
Figure 8. Time averaged charge exchange collision rate.
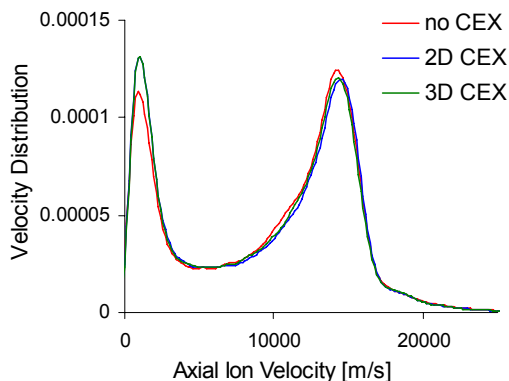
Figure 9. Effect of charge exchange on plasma density distribution at exit plane with scattering (3D) and without scattering (2D).
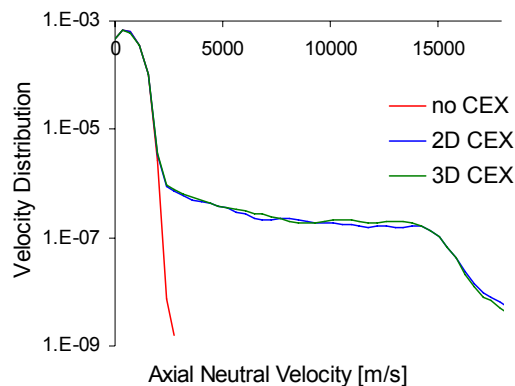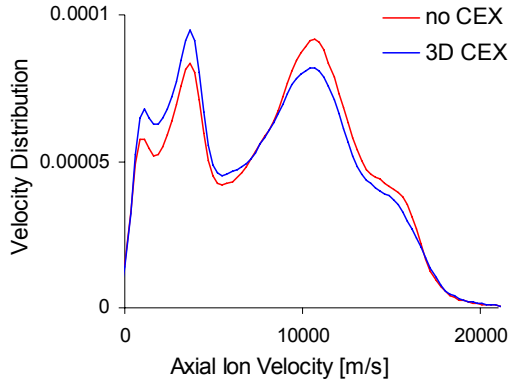

Figure 10. Effect of charge exchange on axial neutral velocity distribution at exit plane with scattering (3D) and without scattering (2D).

For the specific thruster modeled, it was found that charge exchange collisions predominantly occurred half-way along the length of the channel with a higher frequency of collisions along the inner wall as shown in Fig. 8. This location is both upstream of the ionization zone and the region of strong electric field.

As shown by Fig. 9, which includes background gas, adding charge exchange collisions to the simulation reduces the number of high velocity ions and increases the number of low velocity ions. Since the probability of a charge exchange collision between two particles decreases with increasing relative velocity, the change in the distribution is statistically insignificant for ion velocities greater than about 18,000 m/s. The average velocity of the ion population at the exit plane decreases from 9,649 m/s without charge exchange to 9,303 m/s with charge exchange. If the momentum transfer that occurs during a charge exchange collision is not included, then the simulated axial velocity at the exit plane is 9,352 m/s. Therefore, while including charge exchange produces a change of nearly 4% at the exit plane, the effect of scattering during these collisions only produces a 0.5% difference. Experimentally, the average ion velocity at the exit plane is measured to be 9,165 m/s. The simulated value is higher than the experimental value both with and without charge exchange due to the lower simulated voltage at the exit plane.

Since charge exchange decreases the average ion velocity, as expected charge exchange also increases the average neutral velocity as shown in Fig. 10. The average simulated neutral velocity at the exit plane increases from 244 m/s without charge exchange to 271 m/s with 3D charge exchange and 273 m/s with 2D charge exchange. Therefore, charge exchange produces an 11% increase in the neutral velocity at the exit plane. The effect of scattering during charge transfer collisions is still less than 1%. Although the experimental axial neutral velocity at the exit plane is 341 m/s, it is not valid to compare the experimental value with the charge exchange cases. As shown in Fig. 10, rather than shifting the Gaussian peak, charge exchange instead adds a high velocity tail to the velocity distribution. Since the past LIF measurements did not encompass these high velocities, the experimental average would not include such particles. One possible explanation why the experimental value is higher than the simulated values is that the simulated background flux may be too high. Although the pressure is measured to be 0.05 mTorr by an ion gauge at the end of the chamber, it is possible that the actual pressure near the thruster is not equal to this value. If less background gas is present, the average neutral velocity exiting the thruster would increase.

Using the implemented charge exchange model, the effect of these collisions on plasma properties and velocity distributions can be critically examined both in the interior channel and near field region. It is commonly believed that charge exchange may be a significant factor contributing to spacecraft degradation. As suggested by Fig. 11, which does not include background gas, the velocity distribution of particles in the near field region may be very complicated due to the non-uniform acceleration that occurs inside the channel. However, it is clear that the inclusion of charge exchange results in a significant increase in the number of low-energy ions. The probability of an ion having a velocity of 1 km/s increases by 18% due to charge exchange collisions. Note that in reality this probability may be even higher due to the artificially large low-energy population simulated without charge exchange. Collisions also result in a 4% increase in the percentage of population moving slower than 5 km/s. An increase in the number of slow-moving ions is cause for concern, because these particles are more likely to be influenced by stray fields which may be present on an actual spacecraft. If a slow-moving ion is accelerated back towards critical spacecraft components, it could lead to sputtering and deposition.

Figure 11. **Effect of charge exchange on axial ion velocity distribution 1 cm outside thruster at a radial position aligned with outer channel wall .**
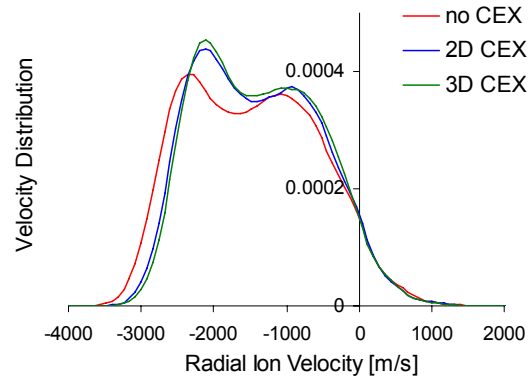
Figure 12. **Effect of charge exchange on radial ion velocity distribution at exit plane at a radial position aligned with inner channel wall.**

The effects of charge exchange collisions on plasma properties in the interior channel of the Hall thruster were more complex than expected. As expected, the backflow of ions toward the anode was reduced due to the impedence added by collisions. Experimentally the backflow is measured to be -230 m/s along the centerline for a 200V discharge voltage. Without collisions, the simulated value was -1200 m/s, while the inclusion of charge exchange reduced the value to -725 m/s. The reason for the large backflow is a simulated electric field upstream of the ionization zone which accelerates the ions back toward the anode. In fact, inclusion of charge exchange collisions caused this reverse field to increase near the anode by 20%. Collisions also resulted in a reduction of electron temperature near the anode of 3%. This lowered temperature in the first 2 to 3 centimeters of the channel, combined with a lowered neutral density in most regions of the channel, results in lower ionization, causing a reduction of the peak plasma density by 2% and a reduction of 55% at the anode. However, although the plasma density is either reduced or remains constant everywhere inside the channel, near the inner wall the neutral density increases by as much as 9% and the peak ionization rate increases by 23%. It is thought that the extra ions produced lead to an increase in the flux of ions to the wall. Upstream of the ionization zone, the radial velocity into the inner wall increases by as much as 50%. However, along the outer wall the radial velocity decreases by as much as 20%. Conversely, beyond the ionization zone, the average radial velocity towards the inner wall decreases as shown in Fig. 12. Along the outer wall, the reverse is true and the average radial velocity increases. The asymmetry observed may be a result of collisional enhancement of asymmetry already present in the thruster. Without collisions, a radial electric field along the centerline of the channel is present which accelerates the ions outward. Since particles with comparable velocities are more likely to collide, this causes charge exchange to occur more frequently along the inner wall. Therefore, the non-uniformity of the collisions leads to a number of slight changes in the plasma which are only indirectly related to the collisions themselves.

IV.   Conclusions

Charge exchange collisions have been included in a 2-D hybrid simulation of the Stanford Hall thruster in order to evaluate the effects of these collisions on velocity distributions and plasma conditions. The charge transfer process was modeled in three dimensions using a rough estimate of the differential cross section in order to assess the impact of scattering that occurs during these collisions. At the exit plane, charge exchange appears to affect the average ion velocity by 4% and the neutral velocity by 11%. Farther downstream, the effect is simulated to be even greater, but the reliability of the simulation near computational boundaries is questionable. However, despite a possible lack of accuracy, an increase in the low-energy population of ions is clearly observed in the near field region, and is possibly significant in understanding spacecraft degradation. In the interior channel of the thruster, the changes induced by charge exchange are typically small, except near the anode, where the code is extremely sensitive to change. Due to a radial non-uniformity in the collision rate, preliminary results suggest the impact of charge exchange on channel wall erosion may have a detrimental effect on the outer wall, and a beneficial effect on the inner wall.

The 29ᵗʰ International Electric Propulsion Conference, Princeton University,
October 31 – November 4, 2005

Acknowledgments

References

[1]Bird, G. A., *Molecular Gas Dynamics and Direct Simulation of Gas Flows*, Oxford University Press, Oxford, 1994, Chap. 11.

[2]Miller, J., Pullins, S., Levandier, D., Chiu, Y. and Dressler, R., "Xenon charge exchange cross sections for electrostatic thruster models," *Journal of Applied Physics,* Vol. 91, No. 3, Feb. 2002, pp. 984.

[3]Gao, R.S., Johnson, L.K., Schafer, D.A., Newman, J.H., Smith, K.A. and Stebbings, R.F., "Absolute differential cross sections for small-angle He^+-He elastic and charge-transfer scattering at keV energies," *Physical Review A,* Vol. 38, No. 6, Sept. 1998, pp. 2789.

[4]Fernandez, E., Cappelli, M. A., Mahesh, K., "2D Simulations of Hall Thrusters," *CTR Annual Research Briefs*, 1998, pp. 81.

[5]Fife, J. M., "Two-Dimensional Hybrid Particle-in-Cell Modeling of Hall Thrusters," S.M. Thesis, Aeronautics and Astronautics Dept., Massachusetts Institute of Technology, Cambridge, MA, 1995.

[6]Fife, J. M., "Nonlinear Hybrid-PIC Modeling and Electrostatic Probe Survey of Hall Thrusters," Ph.D. Dissertation, Aeronautics and Astronautics Dept., Massachusetts Institute of Technology, Cambridge, MA, 1998.

[7]Knoll, A., Gascon, N., Cappelli, M., Fernandez, E., and Kaya, T., "A Two-dimensional (z-theta) Hybrid Simulation of Coaxial Hall Thrusters", IEPC-2005-197, Nov. 2005.

[8]Sommier, E., Allis, M., and Cappelli, M., "Wall Erosion in 2D Hall Thruster Simulation", IEPC-2005-189, Nov. 2005.

[9]Birdsall, C. K, and Langdon, A. B., *Plasma Physics via Computer Simulation*, IOP Publishing Ltd., Briston, England, 1991, Chap. 16.

[10]Siglo Database: http://www.siglo-kinema.com/database/xsect/siglo.sec

[11]Meezan, N. B., Hargus, W. A., and Cappelli, M. A., "Anomalous Electron Mobility in a Coaxial Hall Plasma Discharge," *Physical Review E*, Vol. 63, 026420, 2001.

[12]Thomas, C., Gascon, N., Allis, M., Sommier, E., and Cappelli, M. "Non-Local Electric Field Effects in Magnetized Plasmas", IEPC-2005-028, Nov. 2005.

[13]Dugan, J. V. and Sovie, R. J., "Volume Ion Production Costs in Tenuous Plasmas: A General Atom Theory and Detailed Results for Helium, Argon and Cesium," NASA TN D-4150.

[14]Barral, S., Makowski, K., Peradzynski, Z., Gascon, N., Dudeck, M., "Wall Material Effects in Stationary Plasma Thrusters II: Near-Wall and Inner-Wall Conductivity," *Physics of Plasmas*, Vol. 10, No. 10, Oct. 2003, pp. 4137.

[15]Chen, F., *Introduction to Plasma Physics and Controlled Fusion,* Plenum Press, New York, 1984.

[16]Meezan, N.B., Cappelli, M.A. "Kinetic study of wall collisions in a coaxial Hall discharge" *Physical Review E,* Vol. 66, No. 036401, Sept. 2002.

[17]Cedolin, R.J., "Laser-Induced Fluorescence Diagnostics of Xenon Plasmas," Ph.D. Dissertation, Mechanical Engineering Dept., Stanford University, Stanford, CA, 1997.

[18]Birdsall, C. K, and Langdon, A. B., *Plasma Physics via Computer Simulation*, IOP Publishing Ltd., Briston, England, 1991, Chap. 16.